MODELLING AND SIMULATION OF CHARGE TRANSPORT PHENOMENA IN GRAPHENE ON SIO2 / SI SUBSTRATE AND GRAPHENE ON COMPLEX OXIDE SUBSTRATES

Aditi Kalsh
I.K. Gujral Punjab Technical University, India
E-mail: binti.afa@yahoo.com

V.K. Lamba
I.K. Gujral Punjab Technical University, India
E-mail: lamba_vj@hotmail.com

ABSTRACT

Graphene and silicon are two prominent lithium-ion battery anode materials that have recently received a lot of attention. In this paper, we have modeled and simulated the charge transport phenomena in Graphene on Si / SiO$_2$ and SrTiO$_3$ substrates. The Graphene monolayer's interface with the SrTiO$_3$ (111) surface is analyzed using ab initio density-functional measurements. Both charge and heat flows are produced in solids at the same time when an electrochemical potential is available, bringing about novel properties. The band structure and the electron dissolution process decide the Seebeck coefficient and electrical conductivity. Based on the results acquired, it has been discovered that the interaction of Graphene with SiTiO$_3$ accommodates electronic properties, Seebeck coefficient, and electronic conductivity. For the Graphene / SrTiO$_3$ interface, the best values for the Seebeck coefficient were calculated. This study's findings suggest that the Graphene-SrTiO$_3$ (111) and Graphene-Si structure could exhibit interesting quantum transport behavior.

Keywords: *Complex Oxides, DFT, Lithium-ion battery anode, Modelling*

1. INTRODUCTION

In solids, both charge and heat flows are produced at the same time when an electrochemical potential or a temperature gradient is available, bringing about new properties. The Seebeck coefficient and electrical conductivity are dictated by the band structure and electron dissipating mechanism (Konečný et al., 2018).

We find that the interaction of the Graphene with the SrTiO3 adjusts the electronic properties, the Seebeck coefficient, and the electronic conductivity. Graphene combined with

Si (SiG) is an effective metal-free catalyst for oxygen reduction reactions (ORR) (Chen et al., 2013) and nitrogen monoxide (Chen et al. 2013a; Bhowmik & Rajan, 2022) reduction using density functional theory (DFT) calculations. Theoretically, Si doping in graphene will greatly increase the volume of hydrogen (Cho et al., 2011; Farinre et al., 2022).

Unfortunately, the biggest obstacle to silicon's practical use is a barrier. The anode is known for its large volume shifts during charging and discharging processes, which results in short cycle life and fast fading capacities (Wu & Cui, 2012; Yan et al., 2014; Kueh et al., 2020). To overcome the barrier, an increase in the overall electrochemical efficiency of Si-based anodes in recharging LIBs has been implemented using various methods.

Graphene has sparked a lot of interest because of its two-dimensional (2D) crystal structure with atomic-thickness, unusual electronic structure, high internal mechanical strength, broad surface area, and superior electronic conductivity (Choi et al., 2010; Kim et al., 2022). However, no systematic research on the atomic-scale electrochemical mechanism has been carried out till date.

To facilitate the ever growing demands and to make pace with the rapid advancements in technology, it is required to develop higher order of advanced materials with modified electronic and spin transport properties for development of next-generation devices and various other applications.

In this paper, we study the Charge Transport Phenomena in Graphene on SiO2 / Si Substrate and Graphene on Complex Oxide Substrates with a view to speed the progress in technology.

2. METHODOLOGY

The idea is implemented using Quantum wise ATK software. Using the Quantum wise ATK and the DFT framework, the electronic properties associated with closed and open quantum systems can be modelled. The charge, Spin and Valley Transport in Topological Insulators to design hetero structures and processing on materialized views using Quantum wise ATK software.

Generally, using the linear combination of atomic orbitals (LCAO) basis sets in Quantum wise ATK and the DFT framework, the electronic properties associated with closed and open quantum systems can be modeled. The density matrix, which defines the electron

density is the main factor involved in the self-consistent calculation used in the Kohn–Sham equations.

The Quantum ATK simulation carried out electronic-structure calculations using DFT Hamiltonians, explains reactive empirical force fields in different parameterizations. DFT is carried out using either a plane-wave basis or expansion of electronic states in a LCAO Green's-function methods for electron transport simulations and surface calculations, first-principles electron-phonon and electron-photon couplings, simulation of atomic-scale heat transport, ion dynamics, spintronics and optical properties of materials, static polarization was characterized using Ubuntu Linux 16.04, Quantum espresso, Burai (a GUI of Quantum Espresso) and Vampire.

Quantum ATK charge transport calculations, and Phonon limited mobility of metals carried out. The resistivity of metals is computationally demanding by DFT, to integrate the EPC over both electron and phonon wave vectors (k- and q-space), .Electronic structure of binary alloys, the PPS-PBE method was used with the ATK-LCAO simulation engine (Laughlin, 1981). In the tight-binding method, the elements of the Hamiltonian matrix are treated as adjustable parameters to be fitted to experimental or first-principles calculation results. To estimate the total energy, an additional short-range repulsion term is added to the electronic contribution.

The signature feature of Quantum ATK is used a simulation of device systems. While most DFT device simulation codes are constructed on top of an electronic structure code, Quantum ATK is designed from scratch to achieve the highest accuracy and performance. The NEGF method is used with combination with DFT using pseudo atomic orbitals (PAOs) and pseudo potentials, using a contour integration method, which is based on a continued fraction representation of the Fermi-Dirac function.

The efficiency and accuracy of our implementation are demonstrated by several numerical test calculations on convergence of the density matrix. DFT is a successful theory to calculate the electronic structure of atoms, molecules, and solids. Conventional electronic structure methods attempt to find approximate solutions to the density matrix, which defines the electron density is the main factor involved in the self-consistent calculation used in the Kohn–Sham equations. The Quantum ATK simulation carried out electronic-structure calculations using DFT Hamiltonians, explains reactive empirical force fields in different parameterizations.

s571

3. RESULTS AND DISCUSSION

Modelling and Simulation of Charge Transport Phenomena in Graphene on SiO_2 / Si Substrate and graphene on complex oxide substrates

3.1. Total Energy of Graphene/Si and Graphene/STO

In the geometry optimization procedure, the convergence history per atomic energy concerning the iteration number is plotted. The Graphene/Si Total Energy is shown in Figure 1. The cumulative energy of the Gra/Si is -510.33710764 Ry. Here the 16 iterations were taken, and hence the number of iterations becomes an effective measure of efficiency.

The structure was stable after 16 iterations, as seen in Figure 1; the energy of the equilibrium state after the fifth component is -510.337 eV. SCF is converged between the 1st iteration to 5th iterations. It should be mentioned that forces mobilize faster than energy. When the SCF reaches close convergence, the number of chemical potential iterations becomes 1–2. Geometry optimization exhibits a similar pattern.

The maximum ionic force, maximum ionic displacement, and total energy convergence are Feng Zhou, Ningbo Liao * set tolerance of 0.3000E-01 eV / Å, 0.1000E-02 Å, 0.1000E-04 eV / atom, and calculated results are 2.120132E-002 eV / Å, 4.091334E-004 Å, and 1.597738E-006 eV / atom, respectively.
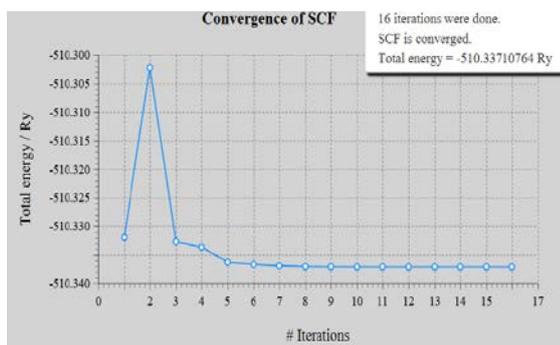
Figure 1: Total energy of the Gra/Si   Figure 1: Phase of geometry optimization of Gra/STO
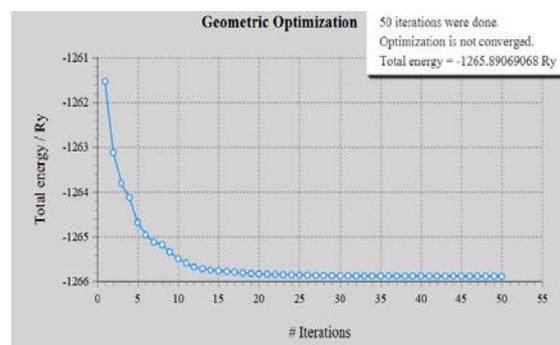
Figure 2 depicts the geometry optimization step of the Gra/STO method, which was completed without any set atoms. The configuration was stable after 50 iterations, as seen in Figure 2, and the total energy of Gra/STO is -1265.89069068 Ry. The equilibrium condition after the 20th iteration has an energy of 1265.890eV, which is not optimized.

3.2. Total force of Graphene/Si and Graphene/STO

s572

The maximal force as a function of iterations is seen in Figure 3. The 50 iterations were recorded here. The plot for a standard DFT run is seen by the black, orange, and grey curves. The black line is the total force of SIG (Graphene/Si). The value of the total force is 0.075896 eV/ Bohr. During the first few stages, the maximal force varies rapidly. The maximum force steadily decreases, although there is some oscillation in the process.

The forces of Si atoms are shown in figure 3 to explain the cause of the oscillation better. Some search direction is tried, but there is an initial dip in forces around iteration 5, but this leads to an increase in energy. Then with a large energy gain, there is a large increase in forces that are due to retardation. There is a small peak in forces 23, and the energy barrier for asymmetric dimerization is overcome as the energy about repetition 23. The force on each atom is reduced to less than 10^{-2}eV / is, and the energy convergence with the energy difference between successive self-sustaining phases is less than 10^{-5} eV. Further, calculate the root-mean-square (RMS) difference between the two quantities to find the difference in force between DFT with and without force correction.
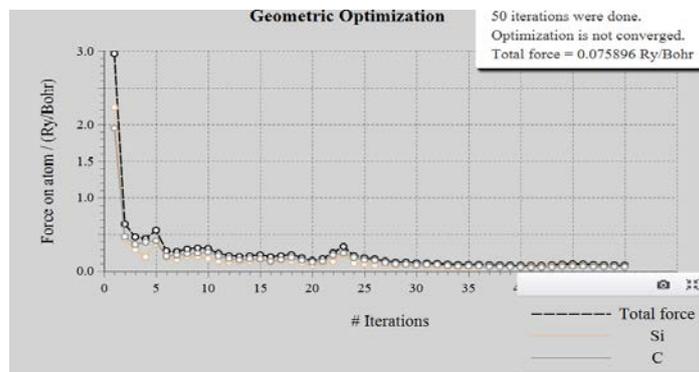
Figure 3: Force on an atom, plotted against the iteration number in geometry optimization.

$$\sqrt{\frac{1}{n}\sum_{i}\left(\frac{F_C^i - F_U^i}{F_C^i}\right)2} \tag{1}$$

Where F_C^i and F_U^i is the corrected and uncorrected forces of the total ionic force at the i-th iteration. The total number of iterations is given as n, and producing these powers is different from the first iteration. From iteration to iteration, the atom with the greatest intensity will change (Roychoudhury et al., 2018; Liu & Luo, 2019).

The stress on the atom is a function of the number of iterations, as seen in Figure 4. In the BFGS model, convergence is achieved after 105 steps of ionic relaxation phases. The overall atomic power correlated with the modified configuration is less than 0.04 eV Å. We

s573

compare the differences in atomic positions and forces obtained from various geometry optimization simulations using the PEXSI method and the diagonal method originating from the same initial position to show the precision of the PEXSI method.

The plot for a regular DFT run is seen by the black, green, grey, red, and dense grey curves. The black lines depict the GRA/STO's total force, while the green, grey, and red colors reflect Sr, Ti, O, and C, respectively. In the third, eighth, and eleventh iterations, small peaks in the powers emerge. The cumulative force is equal to 0.041053 Ry/Bohr.
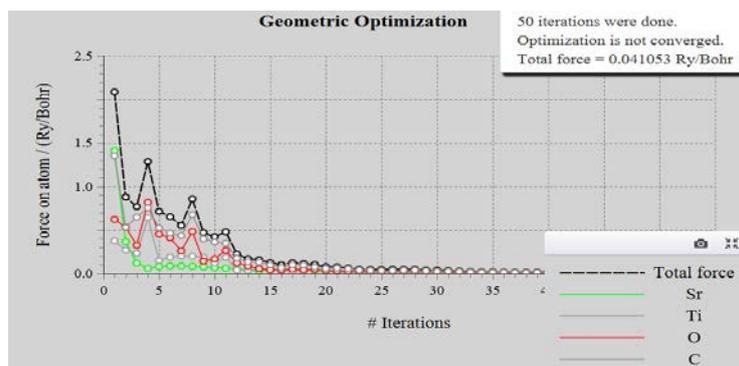
Figure 4: Total force of Graphene/STO

The number of SCF iterations can be used as an absolute measure of computational cost; using atomic variables has a very low computational cost (0.01%).

3.3. Total Stress of Graphene/Si and Graphene/STO

The stress is used to analyze the amount of particulate force that is acting on an element. This makes a path for designing the structure. Methods for visualizing stress propagation in solid materials are useful in a wide range of applications, from architecture to more lightweight structures than implantation techniques on support structures.

Such graphics help us better understand how materials respond to external load conditions and help us build materials with better mechanical properties the standard stresses in the directions where the shear stress components are no longer present. The visualization of stress tensor fields is dependent on these natural stresses, which involve the maximum and minimum normal stress components acting on a point. However, the setting is difficult for a variety of reasons.

This necessitates determining the stress tensor's visual nature to articulate the key stress directions and magnitudes. It entails determining the ratio of principal stresses and various

s574

natural stresses, such as friction and compression. This detail must be formulated concurrently to determine the common variation of the principal stresses in the solid body.

As a scale of topology differences, visualization can provide a global picture of the stress field, conveying a general idea of the main mechanical properties of the body under load and their spatial dependency under various load conditions.
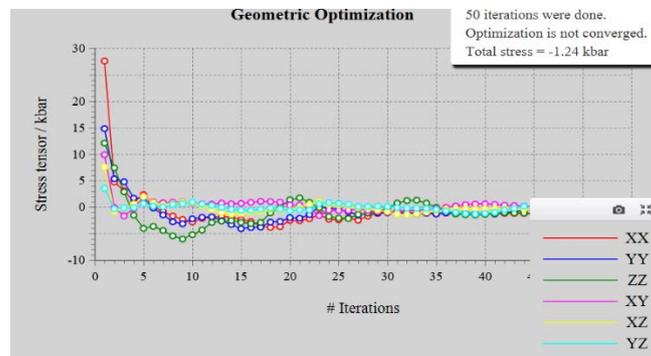
Figure 5: An overview of the optimization process. The objective in the optimization procedure stress versus the number of iterations

Figure 5 Plots of stress tensor against iterations. Here 50 iterations are taken. The various stresses are applied like 28 kbar for red XX,15 kbar for blue YY, 12 kbar for green ZZ, 10 kbar for pink XY, 8 kbar for yellow XZ and 4 kbar aqua YZ colors of lines respectively the changes are noticed. The optimization is not converged, and the value of the total stress is -1.24 kbar. The stress is reached to its minimum value after 30 iterations.
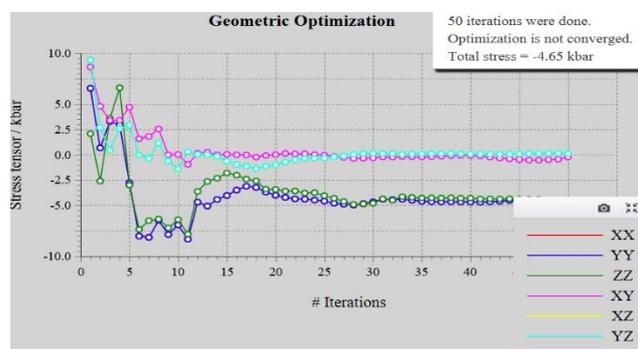
Figure 6: Total stress of Graphene/SrTiO3

Figure 6 show the stress tensor as a function of the number of iterations. Three small peaks in the stress appeared in 6.5 kbar, 5 kbar, and 2.5 kbar in below 10th iterations. The value of the total stress is -4.65 kbar. The stress is reached to its minimum value after 33rd iterations.

3.4.   Molecular Dynamics

s575

MD is a kind of computer simulation in which atoms and molecules interact for a short period. It is difficult to find such complex systems analytically since molecular systems usually contain several particles. Using numerical methods, MD simulation avoids this problem. It serves as a connection between theory and laboratory experiments.

This is referred to as a "virtual experiment." MD simulations are used to study the stability of the C – G structure, which allows single-layer graphene to transform and rotate on a silicon substrate. The original angular orientation has been written in advance. The C – G scheme is depicted schematically in Figure 7 (a).

A 15 nm square-shaped single-layer graphene sheet is positioned on a silicon (001) substrate with dimensions of 25x 25 x4 nm^3 and a (001) core of its surface, the graphene layer of which passes through the center. Graphene is initially positioned above the atomic layer of the silicon (100) board, with an initial orientation angle. Specific graphene is used for different bends with rectangular boundaries set in each direction situation, cutting the edge atomic bonds separately.

The atoms orientation to the silicon surface unit cell is depicted in Figure 7 (b). The angle graph between the armchair vector and the [010] axis (y-axis) (Javvaji et al., 2017; Sun et al., 2021) is used to describe the orientation of graphene. The inter-atomic interactions in the C–G structure are created using the Tersoff and adaptive intermolecular reactive empirical bond ordering (AIREBO) potential functions.
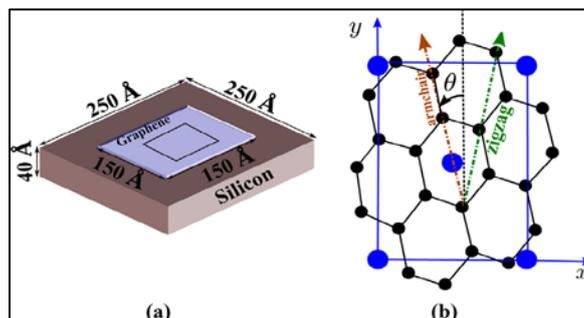
Figure 7: (a) The Si–G system, which was used in MD simulations. (b) Graphene rotation on a silicon substrate with an angle Ө between the armchair orientation and the y-axis.

3.4.1. Total Energy of SIG and Gra/STO

Graphene / Si (SIG) molecular dynamics simulations in the presence and absence of graphene and silicon ions are shown in Figure 8 as a total energy and time plot. After just 0.032

PS, the overall energy versus time profile reaches a plateau, signaling that the simulation has stabilized. The other MD runs' patterns went the same way as these in terms of plateauing. In 0.032 seconds, the cumulative energy reaches -508.4 Ry, then drops to -510.9 Ry. When the cumulative energy standard deviation is less than 0.1, atomic structures of certain time steps are investigated. Time-averaged atomic configurations confirmed the stable interactions in the Si–G system at 300K temperature, length and bond angle analysis. After running 0.10 PS, the overall energy is constant and fluctuates around -510.9 Ry.
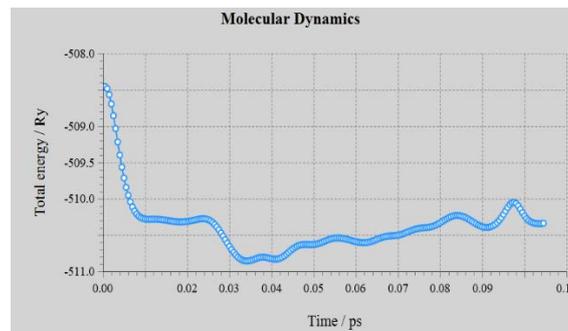
Figure 8: Total energy vs time plot on molecular dynamics of SIG
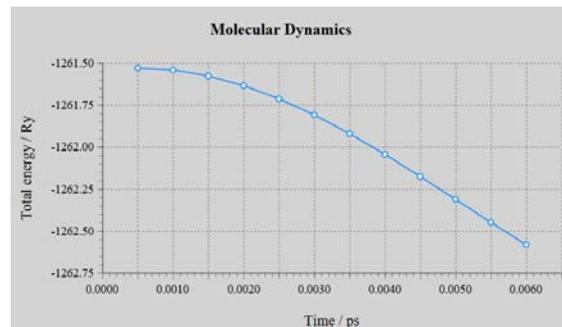
Figure 9: Molecular dynamics simulation showing the total energy of Gra/STO

Figure 9 shows total energy vs time for molecular dynamics simulations of graphene / STO. Total energy changes during 0.0060 ps of simulation time at the equilibrium phase. After running 0.0060 ps, the total energy is constant and fluctuates about -1262.57 Ry, implying that the dynamic structure is essentially stable. The cumulative energy decreases linearly as the time /ps is increased.

Figure10 (a) shows the kinetic energy versus time for the Graphene/Si (SIG) molecular dynamics simulation. The kinetic energy is the same as the total energy reversibly. The maximum kinetic energy is 2.4 Ry, and then the minimum energy is 0 in 0.034 ps of time.

s577
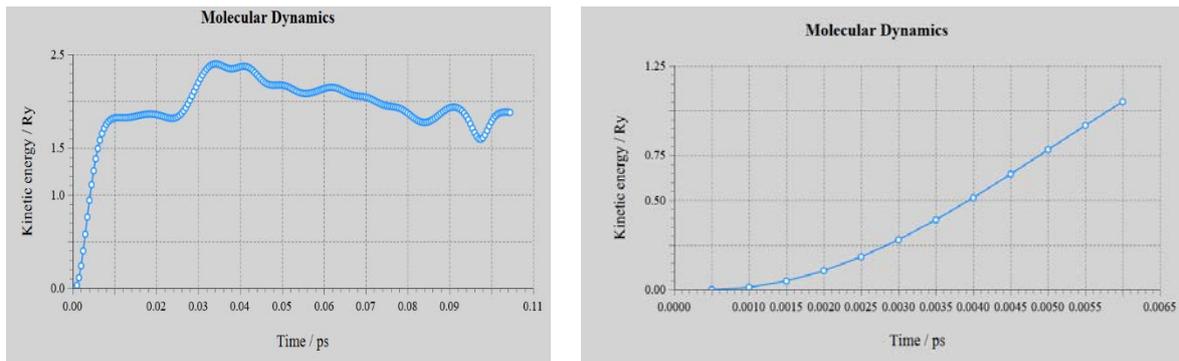
Figure 10: (a) Molecular dynamics simulation of the kinetic energy of Gra/Si (b) Gra/STO

Figure10 (b) shows the kinetic energy of Graphene/STO. When the time is increased, the kinetic energy is increased. The total energy and kinetic energy Analysis of the 1picoseconds The MD trajectory for each complex structure suggest that the complexes were well stabilized at the active site. It may be noted that too much deviation does not indicate that the compounds bind in a better state. The same pattern is obtained for all the total energy, kinetic energy, and temperature of the graph variance. Further analyses suggest that the binding modes of established compounds after MD simulations are almost identical to molecular docking.

Figure11 (a) Represents the temperature vs time of SIG and (b) Gra/STO. The maximum temperature is 4450K in 0.034 Picoseconds of time. Figure 11 (a) followed by equilibration at 4000K. Each successive block of time integration's equilibrium phase significantly redistributes energy locally by significantly lowering individual atoms' thermal velocity, effectively removing numerical artefacts.

The energy for both cooling speeds is roughly equal to the ensemble average. This shows that the cooling mechanism is independent of the cooling rate used in our simulations and produces accurate results. When the device temperature is 4000K, atomic configuration data is used in the definition. The temperature is increased linearly in Figure 11 (b), reaching a mean of 2200 K.
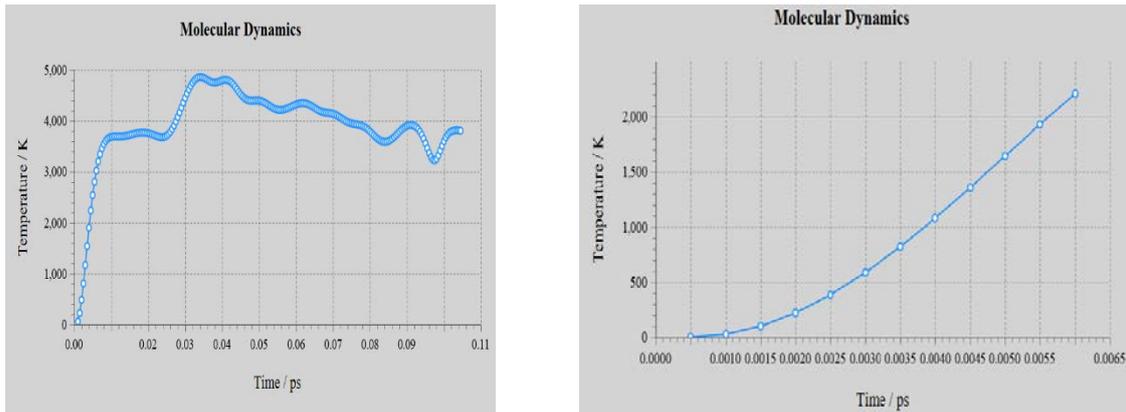
Figure 11: (a) Temperature Impact on SIG and (b) Gra/STO

3.5. Electronic Band Structure

The electronic band structure is the dispersion of electronic energy in the solid's reciprocal space (E-k) relation. It enables us to predict many important properties of solids. The electrons in the valence orbital play a major role in electrical conduction. The promising prospect is the location of Fermi energy, until which all levels are occupied at zero temperature. If the Fermi is located in the energy band gap, it is metallic.

Otherwise, the material is insulating or semiconductor. Bandgap devices play a central role in physics, and a tunable bandgap device can provide great flexibility in design. The band structure of graphene shows very interesting features. The π The electron bands of two-dimensional graphene have linear dispersion valleys and are located at the corners of the hexagon BZ. Two of the valleys are non-equivalent, forming a valley degree of freedom for charge carriers. Due to these characteristics, the charge carrier mass behaves as a Dirac fermion.

Initially, the Gra/ Si hybrid system's geometry was optimized without any fixed atoms on Graphene or Si. Figure 12 depicted the configuration of the Gra/Si scheme.
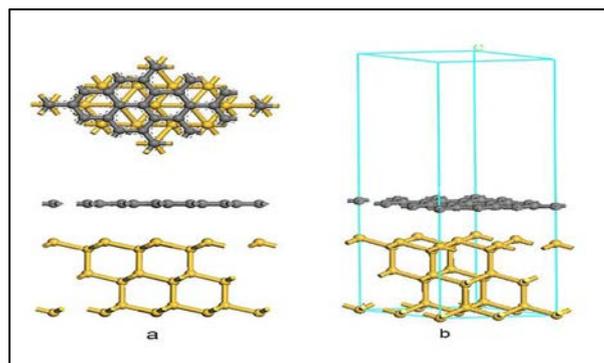
Figure 12: The Gra/Si system structured as : (a) Gra/Si from the top and side view; (b) Gra/Si device unit cell

s579

Figure 13 depicts the band structures of the graphene and Gra/Si frameworks. The Fermi degree is moved to 0 eV in these band structure.
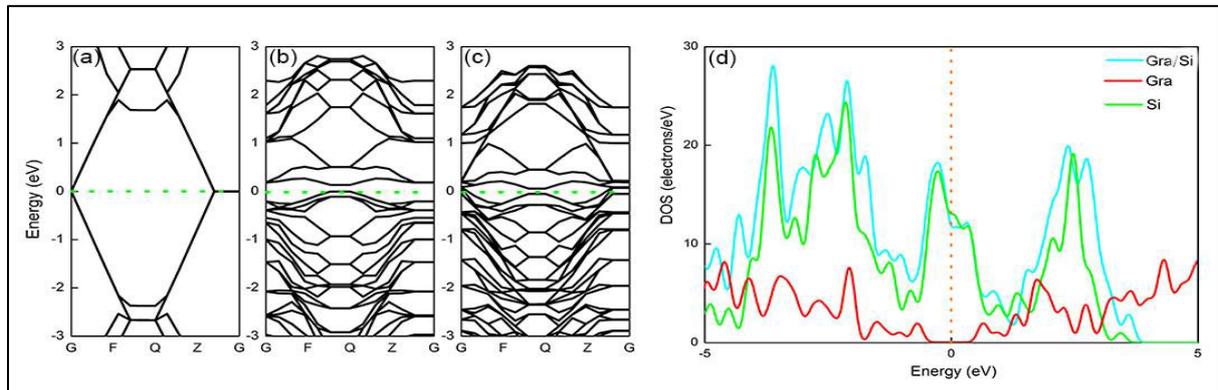
Figure 13: Band structures of (a) graphene, (b) silicon, (c) graphene/silicon, and (d) graphene, silicon, and graphene/silicon DOS.

Figure 14 depicts the electronic density of states (DOS) of graphene/Si in various conditions. A solid black line represents Graphene-Si, Si is represented by an orange line, and a grey line represents C. E =0 denotes the Fermi level's location. The freestanding wave C shows more peaks that mimic van Hove eccentricities in 1D structures and PP π interactions compared to the semi-circular freestanding graphene monolayer with a smooth DOS near EF.

This is due to the lack of natural Ridges. The Davy of the Wavy Si is improved to 7 eV in the broad energy spectrum around the EF, which is significant transport compared to the 6.5 eV wide-bandgap around the EF. The wavy Graphene C (111) surface tends to be attached to a significant DOS enhancement near the EF.
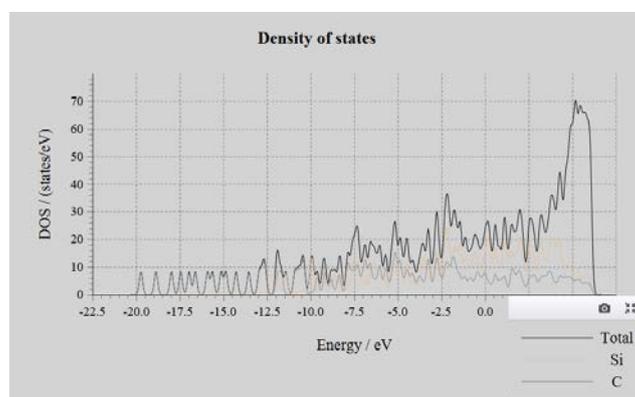
Figure 14: Electronic DOS of wavy graphene-Si

As graphene interacts with the substrate, the fundamental band gap widens to 0.13 eV, equivalent to graphene's contact with other semiconductor surfaces like SiC and Diamond.

s580

According to our Mulliken population analysis, the electron transfer from silicon to graphene is just small.

The interface switches to the PN junction due to this charge redistribution, which is predicted due to the high electronegativity of the C. According to the study, the wavy graphene layer uniformly distributes an additional 0.2 electrons per carbon atom. According to these results, the hybrid Graphene-Si(111) structure would have interesting quantum transport properties.

Graphene/ TiO_2-Terminated STO. The electronic structure of the Ti-STO / Graphene interface is being investigated. Another function is that when graphene interacts with Ti-STO, the graphene canonical point (where the valence band meets the conduction band) is maintained and aligns with the Ti 3d character conduction band minimum (CBM).
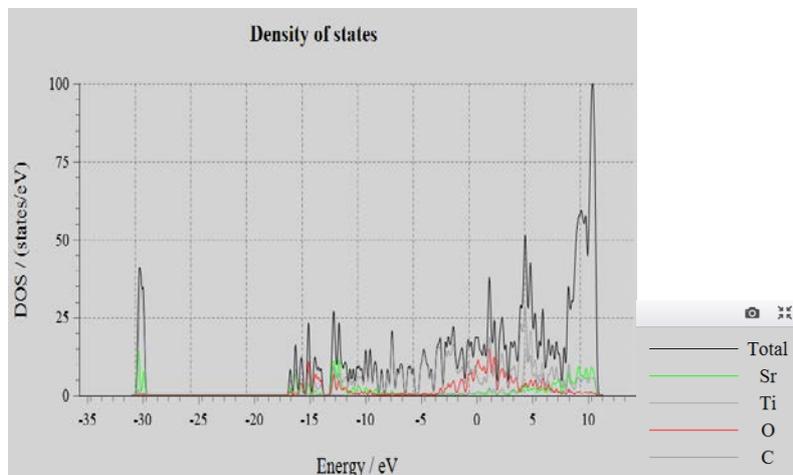
Figure 15: Electronic density of states (DOS) of Graphene/STO

Graphene/SrO-Terminated STO. Our experiment reveal that, compared to Ti-terminated STOs, the structure of contact of graphene sheets is radically different from that of Sr-terminated STOs, as seen in figure 15. In comparison to the high electronic level alignment of graphene on the Ti-STO surface, the graphene electronic level on the ST-STO aligns with the STO surface's limit (VBM), which is governed by the O_2 P-contribution. As a result, the graphene layer interacts with oxygen more strongly than the Ti - STO surface.

The adjustment of STO DOS below the Fermi stage demonstrates this. This is expressed in the graphene layer on Sr-STO having 20 - 40 % higher adsorption energy than Ti-STO. While the graphene canonical point is retained, it has been moved below the Fermi level by 0.5 eV, resulting in efficient n-type doping of the graphene layer, as seen in Figure 15.

s581

It should be remembered that the introduction of STO subsurface oxygen vacancies recently allowed P-type doping, as opposed to graphene sheets on STO. The difference between the work functions will explain the Fermi level shift of graphene, as stated previously. The Fermi amounts of graphene and the substrate are balanced by electron transfer among them.

3.6. Charge transportation of Graphene/Si.

Ab initio density-functional calculations were used to terminate the interface of a graphene monolar with the Al (111) surface. Graphene is not epitaxial for any silicon shell, although silicon and carbon are essentially identical from certain perspectives. The graphene overlayers and the substrate are separated by a huge 11.6 percent lattice on the Si (111) surface, which has the same six-fold symmetry as the graphene overlayers.

Apart from a 0.03 eV broad bandgap around Fermi radiation, graphene's DOS is enhanced to its planer, with a 2 eV wide energy range around EF, essential for transportation. This charge redistribution, which is normally caused by Carbons higher electronegativity compared to Si, transforms the interface into a pn intersection, allowing the extra 0.2 electrons per carbon to be scattered somewhat evenly over the wavy Graphene plate. All of these findings suggest that the Graphene-Si (111) structure may exhibit interesting quantum transport behavior.

4. CONCLUSION

The graphene monolayer's interface with the $SrTiO_3$ (111) surface was terminated using ab initio density-functional measurements. Whereby an electrochemical potential or a temperature differential is present in a solid, both charge and heat flow at the same time, resulting in new properties. The band structure and the electron dissolution process decide the Seebeck coefficient and electrical conductivity. It has been discovered that the interaction of Graphene with $SiTiO_3$ accommodates electronic properties, Seebeck coefficient, and electronic conductivity.

For the Graphene / $SrTiO_3$ interface, the best values for the Seebeck coefficient were 185 V/K. The charge transporters populate the conduction band when chemical potential and temperature rise and the asymmetry of the conduction band causes the transport properties to conduct in opposite directions. All of these findings suggest that the graphene-$SrTiO_3$(111) structure could exhibit interesting quantum transport behavior.

REFERENCES

s582

Bhowmik, S., & Rajan, A. G. (2022). Chemical vapor deposition of 2D materials: A review of modeling, simulation, and machine learning studies. **Iscience**, 103832.

Chen, Y., Yang, X. C., Liu, Y. J., Zhao, J. X., Cai, Q. H., & Wang, X. Z. (2013). Can Si-doped graphene activate or dissociate O2 molecule?. **Journal of Molecular Graphics and Modelling**, 39, 126-132.

Chen, Y., Liu, Y. J., Wang, H. X., Zhao, J. X., Cai, Q. H., Wang, X. Z., & Ding, Y. H. (2013a). Silicon-doped graphene: an effective and metal-free catalyst for NO reduction to N2O?. **ACS applied materials & interfaces**, 5(13), 5994-6000.

Cho, J. H., Yang, S. J., Lee, K., & Park, C. R. (2011). Si-doping effect on the enhanced hydrogen storage of single walled carbon nanotubes and graphene. **international journal of hydrogen energy**, 36(19), 12286-12295.

Choi, W., Lahiri, I., Seelaboyina, R., & Kang, Y. S. (2010). Synthesis of graphene and its applications: a review. **Critical Reviews in Solid State and Materials Sciences**, 35(1), 52-71.

Farinre, O., Mhatre, S. M., Rigosi, A. F., & Misra, P. (2022). Simulation of Graphene Nanoplatelets for NO $ _ {2} $ and CO Gas Sensing at Room Temperature. **arXiv preprint arXiv**:2201.08421.

Kim, H., Kim, Y. D., Wu, T., Cao, Q., Herman, I. P., Hone, J., ... & Shepard, K. L. (2022). Electroluminescence of atoms in a graphene nanogap. **Science Advances**, 8(3), eabj1742.

Konečný, M., Bartošík, M., Mach, J., Švarc, V., Nezval, D., Piastek, J., ... & Šikola, T. (2018). Kelvin probe force microscopy and calculation of charge transport in a graphene/silicon dioxide system at different relative humidity. **ACS applied materials & interfaces**, 10(14), 11987-11994.

Kueh, T. C., Yu, H., Soh, A. K., Wu, H. A., & Hung, Y. M. (2020). Influence of substrate on ultrafast water transport property of multilayer graphene coatings. **Nanotechnology**, 31(37), 375704.

Laughlin, R. B. (1981). Quantized Hall conductivity in two dimensions. **Physical Review B,** 23(10), 5632.

Liu, Y., & Luo, F. (2019). Large-scale highly ordered periodic Au nano-discs/graphene and graphene/Au nanoholes plasmonic substrates for surface-enhanced Raman scattering. **Nano Research**, 12(11), 2788-2795.

Roychoudhury, S., O'Regan, D. D., & Sanvito, S. (2018). Wannier-function-based constrained DFT with nonorthogonality-correcting Pulay forces in application to the reorganization effects in graphene-adsorbed pentacene. **Physical Review B**, 97(20), 205120.

Sun, B., Pang, J., Cheng, Q., Zhang, S., Li, Y., Zhang, C., ... & Zhou, W. (2021). Synthesis of Wafer-Scale Graphene with Chemical Vapor Deposition for Electronic Device Applications. **Advanced Materials Technologies,** 6(7), 2000744.

Wu, H., & Cui, Y. (2012). Designing nanostructured Si anodes for high energy lithium ion batteries. **Nano today**, 7(5), 414-429.

Yan, L., Yang, Y., Zhang, W., & Chen, X. (2014). Advanced materials and nanotechnology for drug delivery. **Advanced Materials**, 26(31), 5533-5540.

s583